

# Conductivities and transport properties of microporous molecular sieves doped composite polymer electrolyte used for lithium polymer battery

Jingyu Xi,<sup>a</sup> Yuxia Bai,<sup>a</sup> Xinping Qiu,<sup>\*a</sup> Wentao Zhu,<sup>a</sup> Liquan Chen<sup>a</sup> and Xiaozhen Tang<sup>b</sup>

<sup>a</sup> Key Lab of Organic Optoelectronics and Molecular Engineering, Department of Chemistry, Tsinghua University, Beijing, 100084, China. E-mail: qiuXP@mail.tsinghua.edu.cn; Fax: +86-10-62794234; Tel: +86-10-62794235

<sup>b</sup> School of Chemistry and Chemical Technology, Shanghai Jiao Tong University, Shanghai, 200240, China

Received (in Montpellier, France) 15th April 2005, Accepted 3rd August 2005  
First published as an Advance Article on the web 15th September 2005

Microporous molecular sieves (MMS), due to their potential for advanced applications in separation technologies, catalysis, and nanoscience, have attracted much attention in the past decades. In this work, a novel PEO-based all solid-state composite polymer electrolyte by using MMS as filler is developed. Thermal analysis and polarized optical microscopy results show that MMS can increase the amount of PEO spherulites and decrease their size, which is beneficial for decreasing the crystallinity of PEO. There exists a much more continuous amorphous phase of PEO in PEO–LiClO<sub>4</sub>/MMS compared with the continuous crystalline phase of PEO in pristine PEO–LiClO<sub>4</sub>, which results in enhancement of ionic conductivity. The excellent lithium transporting properties combined with high decomposition voltage ensures the use of PEO–LiClO<sub>4</sub>/MMS as a candidate electrolyte material for all solid-state rechargeable lithium polymer batteries.

## 1. Introduction

Poly(ethylene oxide)–lithium salt complex (PEO–LiX, X = ClO<sub>4</sub><sup>−</sup>, BF<sub>4</sub><sup>−</sup>, PF<sub>6</sub><sup>−</sup>, CF<sub>3</sub>SO<sub>3</sub><sup>−</sup> *et al.*) based solid polymer electrolytes (SPEs) have received extensive attention,<sup>1–10</sup> for their potential capability to be used as candidate electrolyte materials for rechargeable lithium ion batteries ever since Wright *et al.* found that the complex of PEO and alkaline salts had ionic conductivity ability.<sup>11</sup> The general concept of the transport of Li<sup>+</sup> ions in PEO-based SPEs is coupled with the local relaxation and segmental motion of PEO chains, which conditions can only be obtained when PEO is in its amorphous state.<sup>5</sup> Unfortunately, due to its particular structure, PEO often shows high crystalline ratios at room temperature, resulting in a very low room temperature ionic conductivity ( $\sim 10^{-7}$  S cm<sup>−1</sup>) of PEO-based SPEs,<sup>5,6</sup> which is a drawback for applications in the consumer electronic market such as cell phone and notebook PC.

Development of PEO-based polymer electrolytes capable of combining high ionic conductivity with good mechanical properties is the key problem for the R&D of lithium polymer batteries. When the third component, *i.e.* inorganic fillers, was introduced into the conventional PEO–LiX system to form the composite polymer electrolytes (CPEs), all of the above performances could be improved.<sup>12,13</sup> The inorganic fillers which have been used in CPEs in previous research work can be generally classified into three families: (1) ceramic oxides and/or nanooxides (SiO<sub>2</sub>, Al<sub>2</sub>O<sub>3</sub>, TiO<sub>2</sub>, ZnO, ZrO<sub>2</sub> *et al.*),<sup>14–20</sup> (2) layered clays (montmorillonite *et al.*),<sup>21–23</sup> and (3) ordered mesoporous materials (MCM-41, SBA-15 *et al.*).<sup>24–27</sup> Inorganic fillers help to increase the conductivity of CPEs in two ways:<sup>5,14</sup> (1) increasing the ratios of amorphous phase of PEO, which is of benefit for the transport of Li<sup>+</sup>, by lowering the PEO reorganization tendency; (2) providing Li<sup>+</sup> conducting pathways at the surface regions of the fillers through the

microcosmic interactions, such as Lewis acid–base interactions, among different species in CPEs.

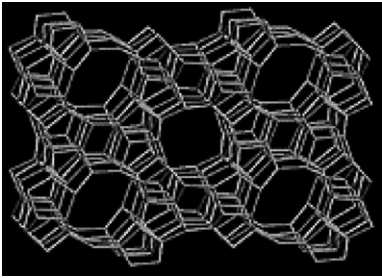
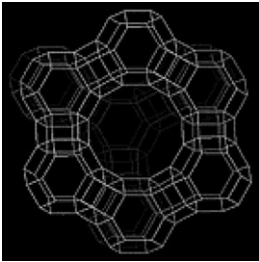
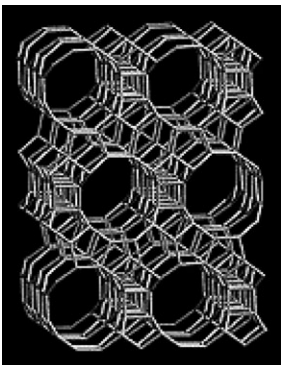
Microporous molecular sieves (MMS)<sup>28,29</sup> and ordered mesoporous materials (OMM)<sup>30–33</sup> have attracted much attention because of their potential for advanced applications in selective absorption and separation technologies, catalysis, electronic engineering, and nanoscience, due to their well-ordered microstructure and special pore size. Porous materials have several advantages compared with traditional ceramic fillers (SiO<sub>2</sub> and Al<sub>2</sub>O<sub>3</sub>), which may influence the lithium transport properties in the CPEs because of their tunable pores/cages size and base/acid sites.<sup>28–33</sup> Furthermore, the cation-exchange centers resulting from the periodic replacement of [AlO<sub>4</sub>]<sup>−</sup> for [SiO<sub>4</sub>] in the framework of MMS means that Li<sup>+</sup> cation can be ion-exchanged into the well-defined channels for charge balance, which may provide novel pathway for the transporting of Li ion. In this work, some microporous molecular sieves (MMS), *i.e.* ZSM-5, Y, and  $\beta$ , were selected to be used as the filler for PEO–LiClO<sub>4</sub> based polymer electrolyte. Electrochemical analysis results show that both ionic conductivity and other electrochemical properties of the resulting CPEs can be greatly enhanced by all three MMS. The enhancement mechanisms of MMS on PEO–LiClO<sub>4</sub> based polymer electrolyte were also studied by differential scanning calorimeter (DSC), infrared spectra, and polarized optical microscopy (POM) techniques.

## 2. Experimental section

### 2.1 Materials

Three types of microporous molecular sieves (MMS) were used, *i.e.* ZSM-5, Y, and  $\beta$ . The framework structure<sup>34,35</sup> and physical properties of above MMS are summarized in Table 1. All MMS samples were obtained from Nankai University Catalyst Company. PEO,  $M_w = 1\,000\,000$  (Shanghai Lian-

**Table 1** Framework structure and physical properties of three microporous molecular sieves

Microporous molecular sieves	Framework type <sup>a</sup>	Framework structure <sup>a</sup>	Pore size (nm) <sup>a</sup>	Average size (nm) <sup>b</sup>	Surface area (m <sup>2</sup> g <sup>-1</sup> ) <sup>c</sup>
ZSM-5	MFI		0.51 × 0.55 [10-ring channel 100] 0.53 × 0.56 [10-ring channel 010]	500	300
Y	FAU		0.74 × 0.74 [12-ring channel 111]	300	400
β	BEA		0.66 × 0.67 [12-ring channel 100] 0.56 × 0.56 [12-ring channel 001]	600	320

<sup>a</sup> See ref. 34 and 35. <sup>b</sup> Evaluated from SEM images. <sup>c</sup> Obtained from BET results.

sheng Chem. Tech. Co. Ltd) and LiClO<sub>4</sub>, A.R. (Shanghai Second Regent Company) were vacuum dried for 24 h at 50 °C and 120 °C, respectively, before use. Acetonitrile, A.R. (Shanghai Chemical Regent Company), dehydrate by 4A molecular sieves before use.

## 2.2 Preparation of composite polymer electrolytes (CPEs)

The preparation of CPEs involved first the dispersion of the MMS powder and LiClO<sub>4</sub> in anhydrous acetonitrile, followed by the addition of the PEO and a thorough mixing of the resulting slurry. The slurry was cast on to a Teflon plate and then the plate was placed into a self-designed equipment, under a sweep of dry air with a flow rate of 10 L min<sup>-1</sup>, in order to let the solvent slowly evaporate. Finally, the resulting films were dried under vacuum at 50 °C for 24 h to get rid of the residual solvent. These procedures yielded translucent homogenous films of thickness about 150 μm (see Fig. 1). The CPEs used in this study were denoted as PEO<sub>10</sub>-LiClO<sub>4</sub>/X%MMS, in which the EO/Li ratio was fixed at 10 : 1 for all samples and the content of MMS, X, ranged from 0 wt.% to 30 wt.% of PEO weight.

## 2.3 Characterization of materials

Differential scanning calorimeter (DSC) measurements were carried out on a Perkin-Elmer Pyris-1 analyzer at a heating rate of 10 °C min<sup>-1</sup>. Polarized optical microscopy (POM) was

performed using a LEICA-DMLP instrument. Infrared spectra were recorded on a PE PARAGN1000 instrument with a wavenumber resolution of 2 cm<sup>-1</sup>.

Ionic conductivity of the composite polymer electrolytes was determined by electrochemical impedance spectroscopy (EIS). The electrolyte was sandwiched between two stainless steel (SS) blocking electrodes to form a symmetrical SS/electrolyte/SS cell. The cell was placed into a self-designed oven coupled with a temperature controller. At each temperature, the cell was allowed to equilibrate for at least 30 minutes before the impedance response was recorded. The impedance tests were carried out in the 1 MHz ~ 1 Hz frequency range using a Solartron 1260 Impedance/Gain-Phase Analyzer coupled with a Solartron 1287 Electrochemical Interface.

Lithium ion transference number, *t*<sub>Li+</sub>, was evaluated using the method of EIS combined with steady-state current technique.<sup>36,37</sup> The electrochemical stability window of the electrolyte was determined by running a linear sweep voltammetry in three-electrode cells using stainless steel as the blocking working electrode, lithium as both the counter and the reference electrodes. A Solartron 1287 Electrochemical Interface was used to run the voltammetry at a scan rate of 1 mV S<sup>-1</sup>.

## 3. Results and discussion

DSC plots of pristine PEO<sub>10</sub>-LiClO<sub>4</sub>, and PEO<sub>10</sub>-LiClO<sub>4</sub>/10%MMS are displayed in Fig. 2. For all samples, the endothermic peak between 20 and 70 °C at heating scan of DSC

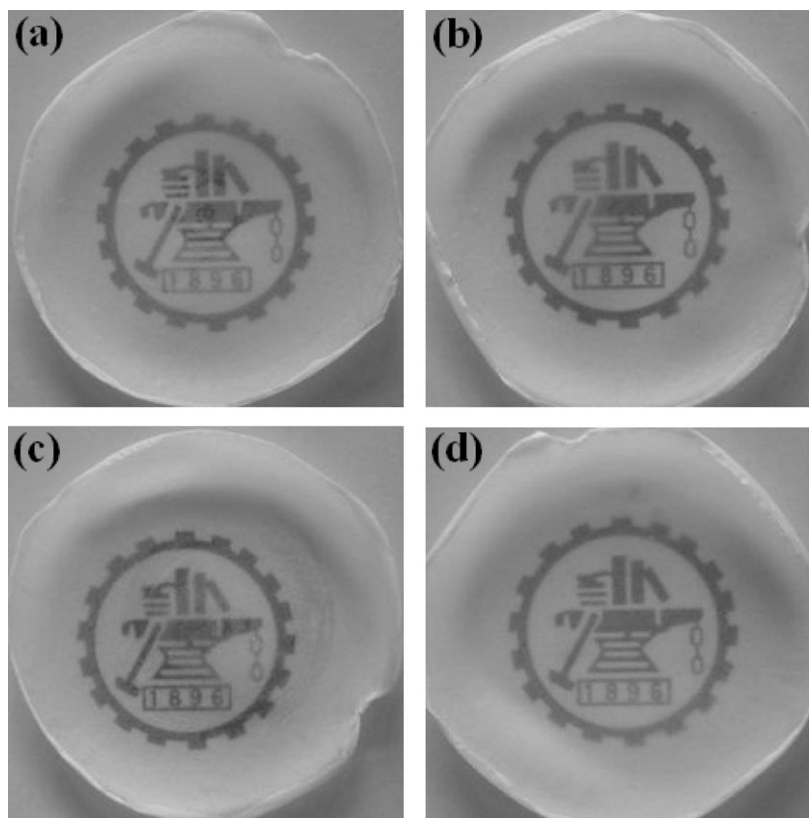


**Fig. 1** Photos of PEO<sub>10</sub>-LiClO<sub>4</sub> (a) and PEO<sub>10</sub>-LiClO<sub>4</sub>/10%MMS composite polymer electrolyte: (b) ZSM-5, (c) Y, (d) β. All films have a diameter of about 5 cm.

curves correspond to the melting of the crystalline PEO. The relative percentage of crystalline PEO,  $X_c$ , can be calculated from the equation  $X_c = \Delta H_m / \Delta H_m^*$ , where  $\Delta H_m^*$  is the melting enthalpy of a completely crystalline PEO sample.<sup>38</sup> The calculated data of  $X_c$  and other thermal properties of all samples are summarized in Table 2.

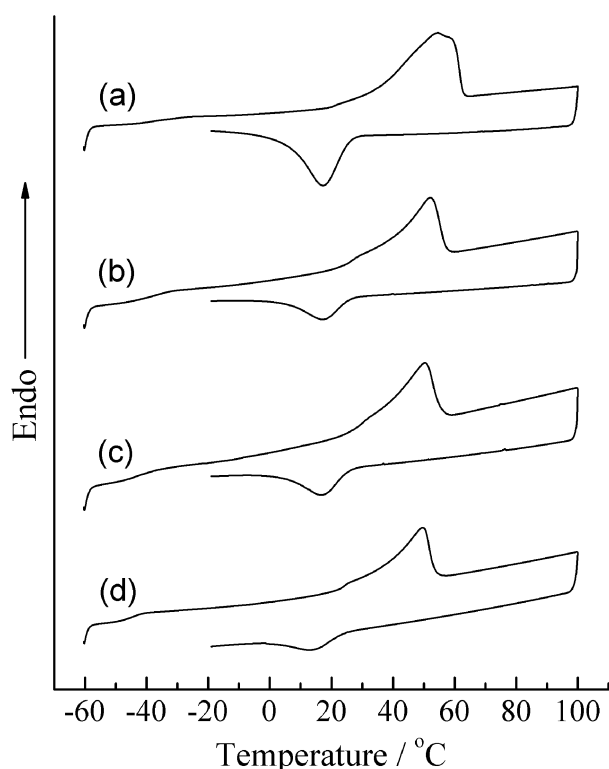


**Fig. 2** DSC curves of PEO<sub>10</sub>-LiClO<sub>4</sub> (a), PEO<sub>10</sub>-LiClO<sub>4</sub>/10%ZSM-5 (b), PEO<sub>10</sub>-LiClO<sub>4</sub>/10%Y (c), and PEO<sub>10</sub>-LiClO<sub>4</sub>/10%β (d).

It can be seen from Fig. 2 and Table 2 that both the melting temperature ( $T_m$ ) and  $X_c$  decrease when MMS is added in PEO<sub>10</sub>-LiClO<sub>4</sub> complex. MMS may decrease the crystallinity of PEO through the Lewis acid–base interactions between the ether O of PEO and Lewis acid sites on the surface of MMS, like the case of ceramic fillers such as SiO<sub>2</sub> and Al<sub>2</sub>O<sub>3</sub>.<sup>5</sup> In addition, all three MMS can also decrease the  $T_g$  of PEO effectively. The decrease of  $T_g$  and  $X_c$  will increase the flexibility of the PEO chains and the ratio of amorphous state PEO, respectively. As a result, the ionic conductivity should be enhanced at low temperature regions.

Fig. 3 shows the temperature dependence of ionic conductivity of pristine PEO<sub>10</sub>-LiClO<sub>4</sub> and PEO<sub>10</sub>-LiClO<sub>4</sub>/10%MMS. All samples show a break around the temperature range of 45 to 60 °C, near the  $T_m$  of PEO (see Fig. 2 and Table 2), reflecting the well-known transition from the PEO crystalline to the amorphous state, which are accompanied by a relevant increase in ionic conductivity. Croce *et al.* suggested that ceramic fillers help to increase the ionic conductivity of CPEs in two ways:<sup>14</sup> (1) increasing the ratios of the amorphous phase of PEO, which is beneficial for the transport of Li<sup>+</sup>; (2) providing special Li<sup>+</sup> conducting pathways at the fillers' surface regions through the Lewis acid–base interactions among different species in the CPEs. The former reason can explain the enhancement of ionic conductivity induced by MMS at the temperature regions lower than  $T_m$  of PEO, consistent with DSC (Table 2) results, which show that MMS can decrease the crystallinity of PEO effectively. On the contrary, the conductivity enhancement at temperature regions higher than the  $T_m$  of PEO should only be attributed to the latter reason that the Lewis acid–base interactions between the Lewis acid sites on the surface of MMS and ether O of PEO chains may provide novel conducting pathway for Li<sup>+</sup>.

Fig. 4 displays the effect of ZSM-5 content on the enhancement of room temperature (25 °C) ionic conductivity of PEO<sub>10</sub>-LiClO<sub>4</sub>/X%ZSM-5. For the case of PEO<sub>10</sub>-LiClO<sub>4</sub>/x%ZSM-5, the enhancement of ionic conductivity first

**Table 2** Thermal properties of pristine PEO<sub>10</sub>-LiClO<sub>4</sub> and PEO<sub>10</sub>-LiClO<sub>4</sub>/10% MMS composite polymer electrolytes obtained from DSC analysis<sup>a</sup>

Sample	Glass point <i>T<sub>g</sub></i> /°C	Melting point <i>T<sub>m</sub></i> /°C	Melting enthalpy $\Delta H_m$ /J g <sup>-1</sup>	Crystallinity <i>X<sub>c</sub></i> <sup>a</sup> /%
PEO <sub>10</sub> -LiClO <sub>4</sub>	-34.8	54.4	83.3	39.0
PEO <sub>10</sub> -LiClO <sub>4</sub> /10% ZSM-5	-41.9	50.4	49.7	23.3
PEO <sub>10</sub> -LiClO <sub>4</sub> /10% Y	-40.3	49.8	51.5	24.1
PEO <sub>10</sub> -LiClO <sub>4</sub> /10% β	-41.5	50.1	50.6	23.7

<sup>a</sup>  $X_c = (\Delta H_m^{\text{sample}}/\Delta H_m^*) \times 100$ ,  $\Delta H_m^* = 213.7 \text{ J g}^{-1}$ .

increases sharply with ZSM-5 content and, at a 10% loading content of ZSM-5, reaches a maximum value that is near one hundred times higher than the pristine PEO<sub>10</sub>-LiClO<sub>4</sub>. When ZSM-5 content is increased further, ionic conductivity decreases. The existence of a maximum value of ionic conductivity indicates that there exist two opposing effects of ZSM-5 on ionic conductivity of PEO<sub>10</sub>-LiClO<sub>4</sub>/x% ZSM-5. The active effect induced by ZSM-5, as mentioned above, can increase the ionic conductivity of the CPEs. On the other hand, when the content of ZSM-5 is too high, the blocking effect on the

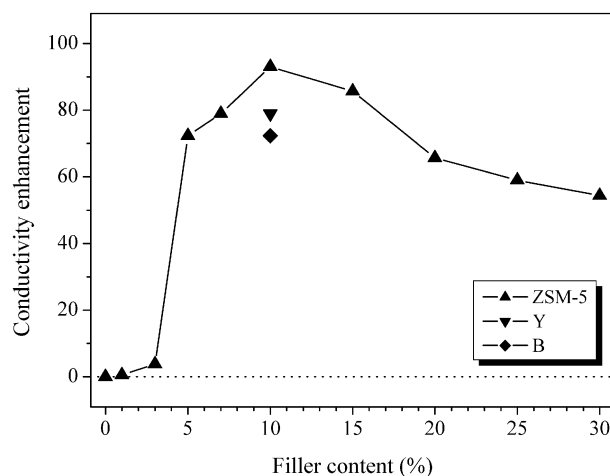


**Fig. 4** Effect of ZSM-5 content on the enhancement of room temperature (25 °C) ionic conductivity of PEO<sub>10</sub>-LiClO<sub>4</sub>/x% ZSM-5 composite polymer electrolytes.

transporting of charge carriers resulting from the aggregating of the ZSM-5, may decrease the ionic conductivity of the CPEs. However, it should be noted that the conductivity decreasing tendency in the case of ZSM-5 is relative small compared with ceramic fillers such as SiO<sub>2</sub> and Al<sub>2</sub>O<sub>3</sub>.<sup>12,13</sup> Interconnecting channels of ZSM-5 (MMS) acting as the conducting pathway of part of the charge carriers may explain this result.

From the above discussions, we have found that MMS can significantly decrease the crystallinity of PEO, and hence improve the room temperature ionic conductivity of PEO-LiClO<sub>4</sub>/MMS composite polymer electrolytes by about two magnitudes. However, it is difficult to understand the effect of MMS on the crystallization kinetics of PEO from only the DSC results. Polarized optical microscopy (POM) is one of the most effective techniques to study the crystallization of PEO and other polymers.<sup>39,40</sup> Fig. 5 displays typical room temperature POM images of pristine PEO<sub>10</sub>-LiClO<sub>4</sub> and PEO<sub>10</sub>-LiClO<sub>4</sub>/10% MMS. It is well known that pure PEO spherulites have a Maltese cross-extinction pattern and a very fine spherulitic texture.<sup>39</sup> For the PEO<sub>10</sub>-LiClO<sub>4</sub> case (Fig. 5a), PEO exhibits a typical compact spherulitic morphology and the cross-extinction pattern can be observed clearly. However, the boundaries of these spherulites are smooth after impingement with adjacent spherulites, in agreement with the results in another paper.<sup>39</sup> In addition, only few spherulites with an average radius of about 50 ~ 100 μm can be observed. It is interesting to note that, with the addition of all three MMS fillers, the amount of PEO spherulites increases and the average radius of spherulites decreases to about 10 μm (Fig. 5b-d). Some MMS particles acting as the nucleus for the growth of PEO spherulites, due to their special microporous structure (see Table 1), may explain this phenomenon. Both the increasing of the amount of PEO spherulites and the decreasing of their size are beneficial for decreasing the crystallinity of PEO, in other words, increasing the ratio of amorphous PEO, as shown in Fig. 6. Compared with the continuous crystalline phase of PEO formed by the connections of adjacent huge PEO spherulites in the case of PEO-LiClO<sub>4</sub> (Fig. 5a and Fig. 6a), there exists a much more continuous amorphous phase of PEO, which is very important for the transporting of Li<sup>+</sup> ions, in PEO-LiClO<sub>4</sub>/MMS composite polymer electrolyte (Fig. 5b-d and Fig. 6b). Further work is however necessary to know how MMS can act as the nucleus of PEO spherulites and isothermal crystallization experiments are currently in progress.

The lithium ion transference number, *t*<sub>Li+</sub>, is one of the important parameters for rechargeable lithium polymer batteries.<sup>1</sup> A relatively high *t*<sub>Li+</sub> can eliminate the concentration

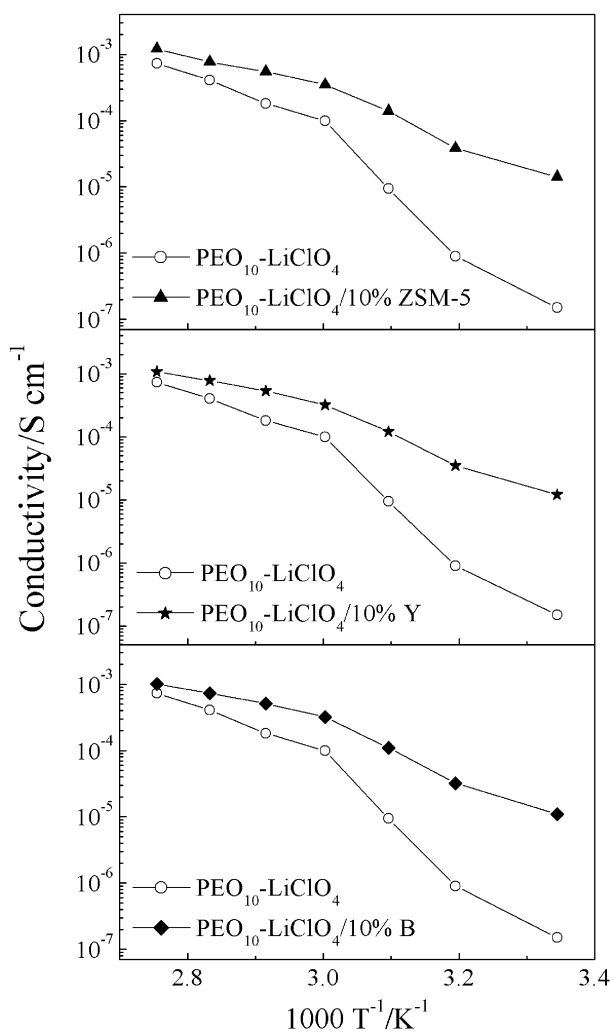


**Fig. 3** Temperature dependence of ionic conductivity of pristine PEO<sub>10</sub>-LiClO<sub>4</sub> and composite polymer electrolytes PEO<sub>10</sub>-LiClO<sub>4</sub>/10% MMS.

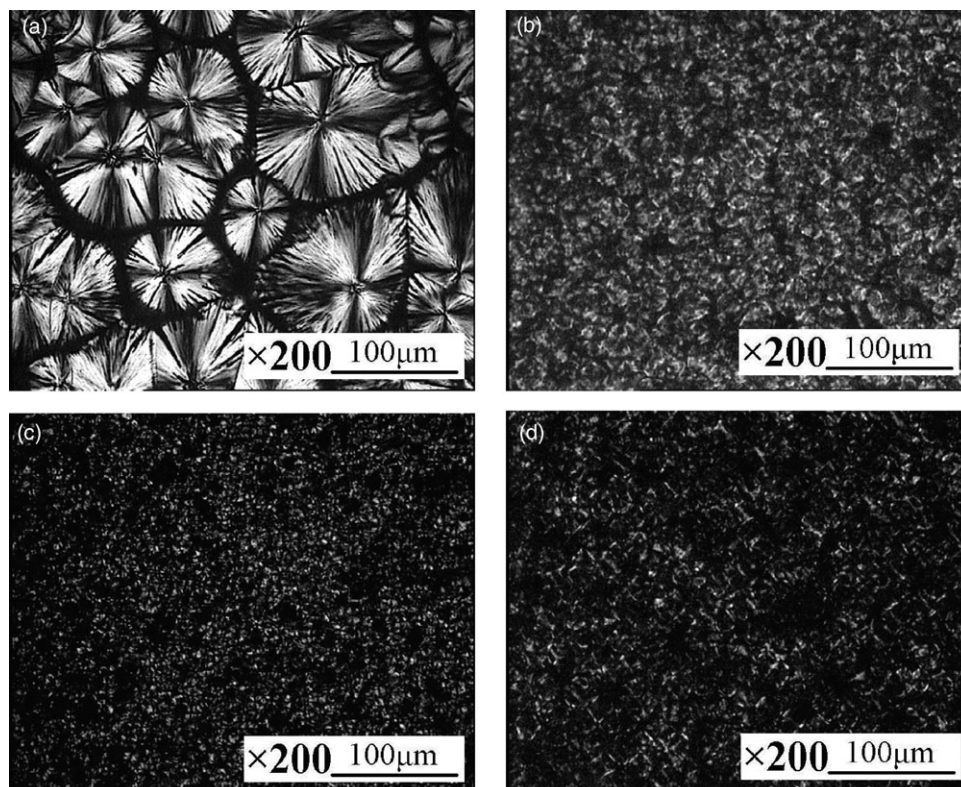


**Fig. 5** Room temperature (25 °C) polarized optical microscopy (POM) images of PEO<sub>10</sub>-LiClO<sub>4</sub> (a), PEO<sub>10</sub>-LiClO<sub>4</sub>/10%ZSM-5 (b), PEO<sub>10</sub>-LiClO<sub>4</sub>/10%Y (c), and PEO<sub>10</sub>-LiClO<sub>4</sub>/10%β (d).

gradients within the battery and can ensure the battery operation under high current density.<sup>1,5</sup> In the case of PEO-LiClO<sub>4</sub>, Li<sup>+</sup> can complex not only with the ether O in PEO but also with the O atoms in ClO<sub>4</sub><sup>-</sup>, and then its transport ability is restricted, resulting in a very low  $t_{\text{Li}^+}$  value (<0.2).<sup>5,14</sup> After the addition of inorganic fillers, such as SiO<sub>2</sub> and Al<sub>2</sub>O<sub>3</sub>,  $t_{\text{Li}^+}$  can be increased slightly through the well-known Lewis acid-base interactions.<sup>5</sup> The Lewis acid sites on the surface of SiO<sub>2</sub> and Al<sub>2</sub>O<sub>3</sub> can interact with O atoms in PEO and ClO<sub>4</sub><sup>-</sup> (Lewis base), and hence weaken the interactions between these O atoms and Li<sup>+</sup>. And as a result, more “free” Li<sup>+</sup> ions are

released and  $t_{\text{Li}^+}$  is enhanced. For PEO-LiClO<sub>4</sub>/MMS composite polymer electrolyte,  $t_{\text{Li}^+}$  can of course be enhanced by the same Lewis acid-base interactions because the framework of MMS is composed of silica and alumina. It can be seen from Table 3 that by the addition of 10% MMS,  $t_{\text{Li}^+}$  of the resulting CPEs were increased to the value of 0.27 ~ 0.35.<sup>5,37</sup>

The FT-IR peak of  $\nu(\text{ClO}_4^-)$  band at the region of 650 to 600 cm<sup>-1</sup> are frequently used to analyze ion-ion interactions in PEO-LiClO<sub>4</sub> based composite polymer electrolytes.<sup>41,42</sup> In the PEO<sub>10</sub>-LiClO<sub>4</sub> (Fig. 7a) case, the peak of  $\nu(\text{ClO}_4^-)$  band split into two peaks at ~624 cm<sup>-1</sup> and ~635 cm<sup>-1</sup>, demonstrates that at least two different kind of ClO<sub>4</sub><sup>-</sup> anions exist in this complex. Salomon *et al.* suggest that the  $\nu(\text{ClO}_4^-)$  band centered between 630 and 635 cm<sup>-1</sup> is associated with the presence of Li<sup>+</sup>-ClO<sub>4</sub><sup>-</sup> contact-ion pairs whereas the band centered at about 623 cm<sup>-1</sup> can be attributed to free ClO<sub>4</sub><sup>-</sup> anions.<sup>41</sup> As can be seen from Fig. 7b, the peak characteristic for “free” ClO<sub>4</sub><sup>-</sup> is much larger than that of contact-ion pairs. This is because that the relative low content of LiClO<sub>4</sub> (O/Li = 10) is helpful for its dissolving in the PEO matrix. For CPEs containing MMS, the peak characteristic to contact-ion pairs at ~635 cm<sup>-1</sup> becomes even smaller and only a trace shoulder peak corresponding to contact-ion pairs can be found (Fig. 7b-d), suggesting that the ratio of free Li<sup>+</sup> increases with

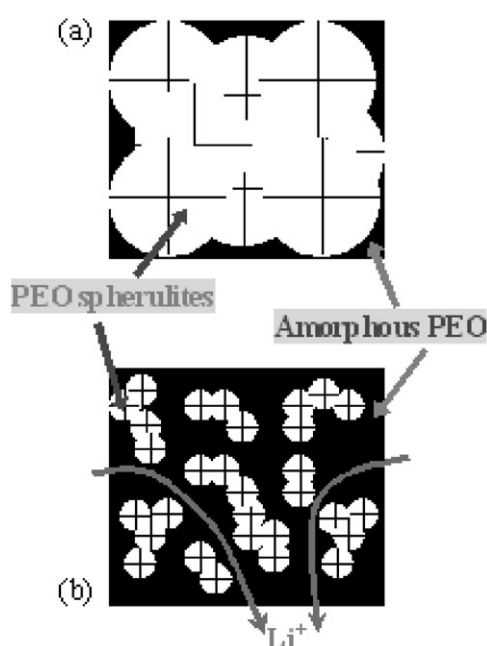


**Fig. 6** Schematic representation of PEO spherulites in pristine PEO-LiClO<sub>4</sub> (a) and composite polymer electrolyte PEO-LiClO<sub>4</sub>/MMS (b).

**Table 3** Lithium ion transference number ( $t_{\text{Li}^+}$ ) of pristine PEO<sub>10</sub>-LiClO<sub>4</sub> and PEO<sub>10</sub>-LiClO<sub>4</sub>/10% filler composite polymer electrolytes

Sample	$t_{\text{Li}^+}$
PEO <sub>10</sub> -LiClO <sub>4</sub>	0.19
PEO <sub>10</sub> -LiClO <sub>4</sub> /10%SiO <sub>2</sub>	0.24 <sup>a</sup>
PEO <sub>10</sub> -LiClO <sub>4</sub> /10%Al <sub>2</sub> O <sub>3</sub>	0.25 <sup>a</sup>
PEO <sub>10</sub> -LiClO <sub>4</sub> /10%ZSM-5	0.35
PEO <sub>10</sub> -LiClO <sub>4</sub> /10%Y	0.27
PEO <sub>10</sub> -LiClO <sub>4</sub> /10%β	0.28

<sup>a</sup> Data obtained from ref. 37.

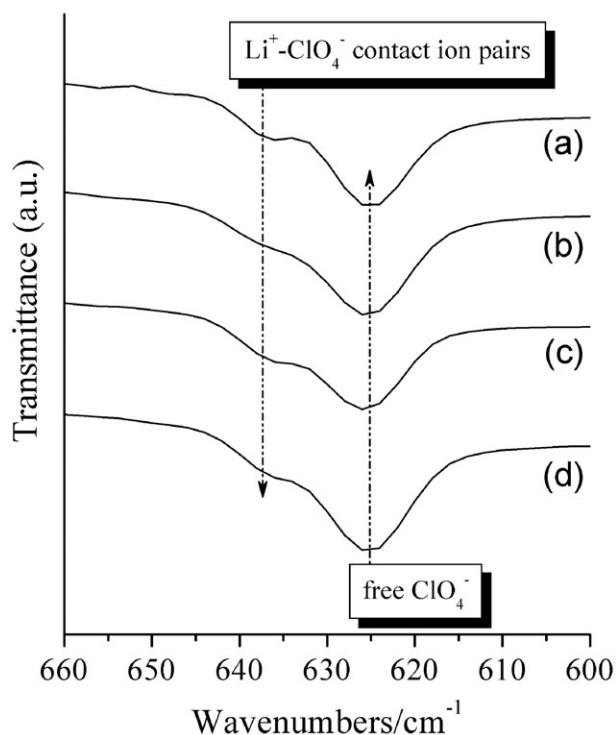


**Fig. 7** FT-IR spectra in the wavenumber range of 660  $\text{cm}^{-1}$  to 600  $\text{cm}^{-1}$ . (a)  $\text{PEO}_{10}\text{-LiClO}_4$ ; (b)  $\text{PEO}_{10}\text{-LiClO}_4/10\%\text{ZSM-5}$ ; (c)  $\text{PEO}_{10}\text{-LiClO}_4/10\%\text{Y}$ ; (d)  $\text{PEO}_{10}\text{-LiClO}_4/10\%\beta$ .

the addition of MMS, consistent with the results in Table 3 that  $t_{\text{Li}^+}$  values of  $\text{PEO}_{10}\text{-LiClO}_4/10\%\text{MMS}$  are higher than that of  $\text{PEO}_{10}\text{-LiClO}_4$ .

Fig. 8 presents the linear voltage sweep curves of pristine  $\text{PEO}_{10}\text{-LiClO}_4$  and  $\text{PEO}_{10}\text{-LiClO}_4/10\%\text{MMS}$  composite poly-

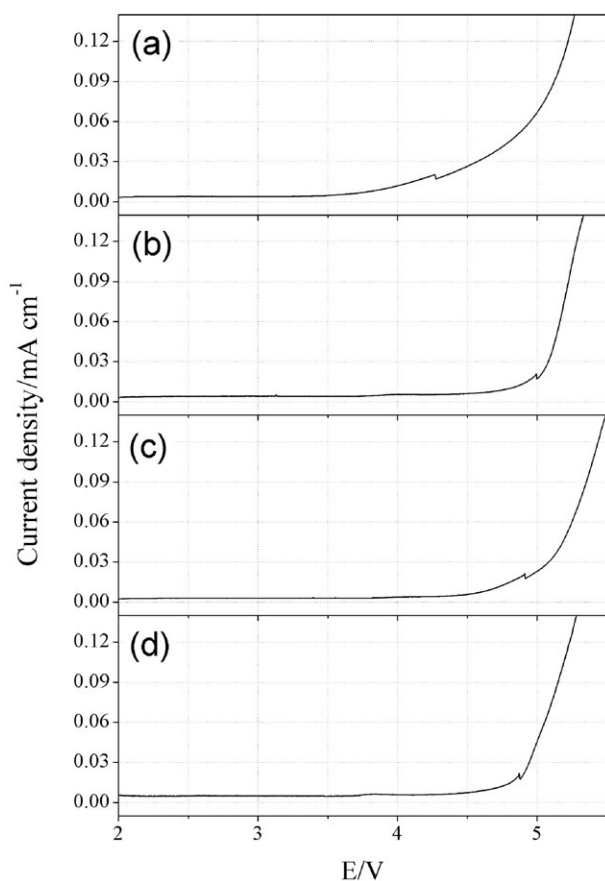


**Fig. 8** Current-voltage response of pristine  $\text{PEO}_{10}\text{-LiClO}_4$  and  $\text{PEO}_{10}\text{-LiClO}_4/10\%\text{MMS}$  composite polymer electrolytes at 90  $^{\circ}\text{C}$ .

mer electrolytes. The irreversible onset of the current determines the electrolyte breakdown voltage, which in the case of  $\text{PEO}_{10}\text{-LiClO}_4$  extends to about 3.8 V vs. Li (Fig. 8a). After the addition of all three MMS, the decomposition voltage of the resulting  $\text{PEO}_{10}\text{-LiClO}_4/10\%\text{MMS}$  increased and exceed 4.5 V vs. Li (Fig. 8b-d), which should be attributed to the interaction between MMS and PEO chains. The above results suggest that  $\text{PEO-LiClO}_4/\text{MMS}$  composite polymer electrolytes can be used as candidate electrolyte materials for rechargeable lithium polymer batteries whose working voltage is higher than 4.5 V.

## 4. Conclusions

A novel PEO-based all solid-state composite polymer electrolyte has been obtained using microporous molecular sieves (MMS) as filler. Thermal analysis and polarized optical microscopy results show that MMS can increase the amount of PEO spherulites and decrease their size, which is beneficial for decreasing the crystallinity of PEO. Compared with the continuous crystalline phase of PEO in pristine  $\text{PEO-LiClO}_4$ , there exists much more continuous amorphous phase of PEO in  $\text{PEO-LiClO}_4/\text{MMS}$ , resulting in significant enhancement of ionic conductivity. In addition, MMS can also enhance the lithium ion transference number of the CPEs slightly. The excellent lithium transporting properties combined with high decomposition voltage ensures the use of  $\text{PEO-LiClO}_4/\text{MMS}$  as candidate electrolyte material for all solid-state rechargeable lithium polymer batteries.

## Acknowledgements

This work was supported by the State Key Basic Research Program of China (2002CB211803) and Key Science and Technology Project of Shanghai (02dz11002).

## References

- 1 J. M. Tarascon and M. Armand, *Nature*, 2001, **414**, 359.
- 2 W. H. Meyer, *Adv. Mater.*, 1998, **10**, 439.
- 3 V. Chandrasekhar, *Adv. Polym. Sci.*, 1998, **135**, 139.
- 4 F. M. Gray, *Polymer Electrolytes*, Royal Society of Chemistry, Cambridge, 1997.
- 5 F. Croce, G. B. Appetecchi, L. Persi and B. Scrosati, *Nature*, 1998, **394**, 456.
- 6 B. Scrosati, F. Croce and S. Panero, *J. Power Sources*, 2001, **100**, 93.
- 7 Z. Gadjourova, Y. G. Andreev, D. P. Tunstall and P. G. Bruce, *Nature*, 2001, **412**, 520.
- 8 Z. Stoeva, I. M. Litas, E. Staunton, Y. G. Andreev and P. G. Bruce, *J. Am. Chem. Soc.*, 2003, **125**, 4619.
- 9 A. M. Christie, S. J. Lilley, E. Staunton, Y. G. Andreev and P. G. Bruce, *Nature*, 2005, **433**, 50.
- 10 C. W. Nan, L. Z. Fan, Y. H. Lin and Q. Cai, *Phys. Rev. Lett.*, 2003, **91**, 266104.
- 11 D. E. Fenton, J. M. Parker and P. V. Wright, *Polymer*, 1973, **14**, 589.
- 12 E. Quartarone, P. Mustarelli and A. Magistris, *Solid State Ionics*, 1998, **110**, 1.
- 13 J. Zhou and P. S. Fedkiw, *Solid State Ionics*, 2004, **166**, 275.
- 14 F. Croce, R. Curini, A. Martinelli, L. Persi, F. Ronci and B. Scrosati, *J. Phys. Chem. B*, 1999, **103**, 10632.
- 15 F. Croce, L. Persi, B. Scrosati, F. Serraino-Fiory, E. Plichta and M. A. Hendrickson, *Electrochim. Acta*, 2001, **46**, 2457.
- 16 H. M. Xiong, X. Zhao and J. S. Chen, *J. Phys. Chem. B*, 2001, **105**, 10169.
- 17 S. Zhang, J. Y. Lee and L. Hong, *J. Power Sources*, 2004, **126**, 125.
- 18 M. A. K. L. Dissanayake, P. A. R. D. Jayatilaka, R. S. P. Bokalawala, I. Albinsson and B. E. Mellander, *J. Power Sources*, 2003, **119-121**, 409.
- 19 M. Nookala, B. Kumar and S. Rodrigues, *J. Power Sources*, 2002, **111**, 165.
- 20 J. Y. Xi and X. Z. Tang, *Chem. Phys. Lett.*, 2004, **393**, 271.
- 21 L. Z. Fan, C. W. Nan and M. Li, *Chem. Phys. Lett.*, 2003, **369**, 698.
- 22 R. A. Vaia, S. Vasudevan, W. Krawiec, L. G. Scanlon and E. P. Giannelis, *Adv. Mater.*, 1995, **7**, 154.

- 23 G. Sandí, K. A. Carrado, H. Joachin, W. Q. Lu and J. Prakash, *J. Power Sources*, 2003, **119–121**, 492.
- 24 P. P. Chu, M. J. Reddy and H. M. Kao, *Solid State Ionics*, 2003, **156**, 141.
- 25 M. J. Reddy and P. P. Chu, *J. Power Sources*, 2004, **135**, 1.
- 26 J. Xi, X. Qiu, X. Ma, M. Cui, J. Yang, X. Tang, W. Zhu and L. Chen, *Solid State Ionics*, 2005, **176**, 1249.
- 27 J. Y. Xi and X. Z. Tang, *Chem. Phys. Lett.*, 2004, **400**, 68.
- 28 A. Corma, *Chem. Rev.*, 1997, **97**, 2373.
- 29 C. S. Cundy and P. A. Cox, *Chem. Rev.*, 2003, **103**, 663.
- 30 J. Y. Ying, C. P. Mehnert and M. S. Wong, *Angew. Chem. Int. Ed.*, 1999, **38**, 56.
- 31 A. Stein, B. J. Melde and R. C. Schrodén, *Adv. Mater.*, 2000, **12**, 1403.
- 32 X. He and D. Antonelli, *Angew. Chem. Int. Ed.*, 2002, **41**, 214.
- 33 J. L. Shi, Z. L. Hua and L. X. Zhang, *J. Mater. Chem.*, 2004, **14**, 795.
- 34 Ch. Baerlocher, W. M. Meier and D. H. Olson, *Atlas of Zeolite Framework Types*, 5th edn., Elsevier, Amsterdam, 2001.
- 35 <http://www.iza-structure.org/databases/>.
- 36 P. G. Bruce and C. A. Vincent, *J. Electroanal. Chem.*, 1987, **225**, 1.
- 37 J. Xi, X. Ma, M. Cui, X. Huang, Z. Zheng and X. Tang, *Chin. Sci. Bull.*, 2004, **49**, 785.
- 38 X. Li and S. L. Hsu, *J. Polym. Sci. Polym. Phys. Ed.*, 1984, **22**, 1331.
- 39 B. Choi, *Solid State Ionics*, 2004, **168**, 123.
- 40 A. Ziabicki and B. Misztal-Faraj, *Polymer*, 2005, **46**, 2395.
- 41 M. Salomon, M. Xu, E. M. Eyring and S. Petrucci, *J. Phys. Chem.*, 1994, **98**, 8234.
- 42 W. Wiczkorek, D. Raducha, A. Zalewska and J. R. Stevens, *J. Phys. Chem. B*, 1998, **102**, 8725.